Research Article | Vol. 30, No. 13 / 20 Jun 2022 / Optics Express 22830
Optics EXPRESS

Near-infrared narrow-band minus filter based on a Mie magnetic dipole resonance

KAI WANG,[1,2] YING XIONG,[1,2] QIANG LI,[1] YANCHAO WANG,[1] JIAN ZHANG,[1] HAI LIU,[1] ZHEN LIU,[1] TONGTONG WANG,[1] ZHENFENG SHEN,[1] XIAOKUN WANG,[1] XIAOYI WANG,[1] JINSONG GAO,[1,3] AND HAIGUI YANG[1,*]

[1]*Key Laboratory of Optical System Advanced Manufacturing Technology, Changchun Institute of Optics, Fine Mechanics and Physics, Chinese Academy of Sciences, Changchun 130033, China*
[2]*University of the Chinese Academy of Sciences, Beijing 100039, China*
[3]*Jilin Provincial Key Laboratory of Advanced Optoelectronic Equipment and Instrument Manufacturing Technology, Changchun 130033, China*
[*]*yanghg@ciomp.ac.cn*

Abstract: The traditional minus filter is composed of many layers of thin films, which makes it difficult and complicated to manufacture. It is sensitive to incident light angle and polarization. Here, we propose a near-infrared narrow-band minus filter with a full width at half maximum around 5 nm made of all-dielectric Si-SiO_2 structures without any ohmic loss. The stop band transmittance of the proposed filter is close to 0, while its broad pass band transmittance is as high as 90% in the work wavelength range. Theoretical analysis shows that the transmission dip originated from magnetic dipole resonance: Its position can be tuned from 1.3 μm to 1.8 μm by changing the thickness of Si structure, and the proposed structure is insensitive to changes in incident light angle and polarization angle. We further studied its potential applications as a refractive index sensor. The sensitivity of dip1 and dip2 are as high as 953.53 nm/RIU and 691.09 nm/RIU, while their figure of merit is almost unchanged: 59.59 and 115.18, respectively.

1. Introduction

Minus filters, also called notch filters, pass most wavelengths almost lossless while attenuating the specified wavelength band (stop band) [1]. Minus filters are applied in various fields [2] including image processing [2], data transmission, seismology [3], biomedical engineering [4,5], Raman spectroscopy, and laser protective coatings [6–9]. High and low refractive index film stacks with refractive index differences are a traditional way to design minus filters. The width of the stop band depends on the ratio of the refractive indices and thickness of the high and low index layers [1]. The width of the stop band is controlled by choosing a relatively small difference of index refraction between two materials. However, it is still difficult to identify two materials with appropriate high and low indexes and then precisely control their thickness for a narrow-band minus filter. Additionally, traditional filters are sensitive to changes in incident light angle and polarization angle.

Metamaterials [10–14] are artificial materials gaining significant attention due to their small volume, simple fabrication, and low losses. Plasmonic-based metamaterials including nano-holes [15–19] and metal-insulator-metal arrays [20–22] have been demonstrated as color filters and infrared filter devices. However, the metals used in plasmonic structures have intrinsic loss that leads to lower efficiency at optical frequencies. All dielectric-based structures are favored because of their low losses in compared to plasmonic structures. Recently, various all-dielectric optical filters [23–25] have been widely studied including color filters and reflection filters based on silicon, germanium, and other high refractive index materials. However, a minus filter with low sideband and narrow high-efficiency blocking at the stop-band are still expected [26].

#454541 https://doi.org/10.1364/OE.454541
Journal © 2022 Received 16 Feb 2022; revised 20 Mar 2022; accepted 11 Apr 2022; published 8 Jun 2022

Optics EXPRESS

Here, we propose a narrowband minus filter with high-efficiency blocking in the near-infrared region made of all dielectric metamaterials. The system was designed using a two-layer structure of Si-SiO_2. The Si-layer is composed of clusters containing four identical subwavelength high-index dielectric nanoblocks, i.e., diamond in cross-section with rhombic shapes. A full width at half maximum (FWHM) of this filter is as low as 5 nm. The position of the stop band of the minus filter does not change with the angle of the incident light and polarization. By changing the thickness of the Si structure, the position of stop band can be tuned from 1.3 μm to 1.8 μm, which facilitates the design of the narrow minus filter in the near-infrared. This structure can also be used to design near-infrared reflection filters and maintain the same excellent performance. The refractive index (RI) can be used for high sensitivity sensor applications.

2. Simulations

A schematic of the proposed minus filter based on dielectric metamaterials is shown in Fig. 1. This minus filter is designed by a two-layer structure of Si-SiO_2. The bottom left of Fig. 1 shows details of the unit cell. The unit of minus filter is composed of clusters containing four identical subwavelength high-index dielectric nanoblocks that are diamond-shaped in cross-section with rhombic shapes. The period p is 1.1 μm. the length a and l are 0.21 μm and 0.55 μm. The thickness of the nanoblocks is 0.5 μm. We used a finite difference time-domain (FDTD) algorithm to analyze the optical proprieties of proposed minus filter and set periodic boundary conditions along x and y directions; perfectly matched layers were selected in the z direction. The permittivity values of Si and SiO_2 in the analysis were derived from Palik [27]. In the simulation, the proposed negative filter is illuminated by the normal incident plane wave with electric field amplitude E0 and magnetic field amplitude H0 along the negative direction of Z axis, and the polarization direction of plane wave is along the X axis. The mesh accuracy was set to 5 nm to ensure simulation precision.

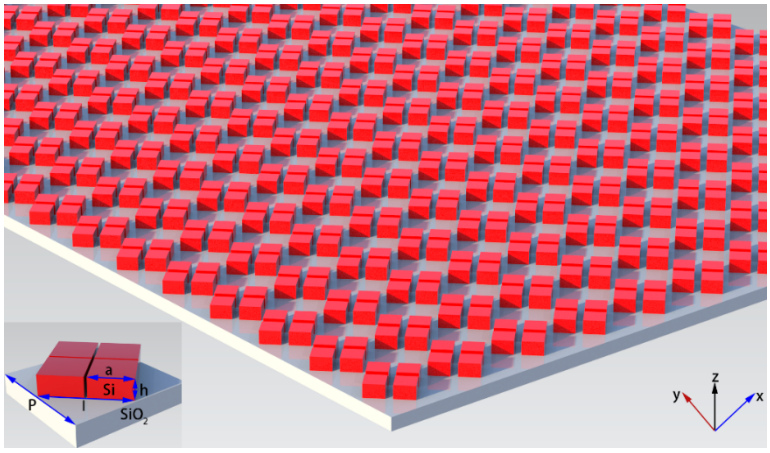

Fig. 1. Proposed structure based on dielectric metamaterials. The illustration and geometric of a unit cell in the lower left corner light with x-polarization is normally incident along the negative direction of the z-axis.

At the same time, we also analyze the feasibility of the experimental manufacture of the proposed minus filter. The manufacturing process of the proposed minus filter is well compatible with the traditional complementary metal-oxide-semiconductor (CMOS) technology. Firstly, silicon thin films are deposited on silica structure by plasma-enhanced chemical-vapor-deposition (PECVD) technology. Then we spin-coat a layer of photoresist on the surface of the silicon film.

Optics EXPRESS

Next, electron beam lithography (EBL), direct laser writing (DLW) and inductively coupled plasma etching (ICP) are used to obtain the required minus filter.

Figure 2 shows simulated transmission spectrum of the proposed minus filter when the thickness of the nanoblocks is 0.5 μm, p = 1.1 μm, a = 0.21 μm, and l = 0.55 μm. We conclude from the transmission spectrum that the specified wavelength bands (at 1.5 μm) are attenuated to nearly zero corresponding to a stop band in the minus filter. The FWHM of the stop band is just 5 nm; other wavelengths can be maintained to above 90%. The optical response of the proposed structure is good for designing the minus filter. In addition, the FWHM of reflection spectrum is also just 5 nm, and thus this structure can also be used to design near-infrared reflection filters and maintain the same excellent performance.

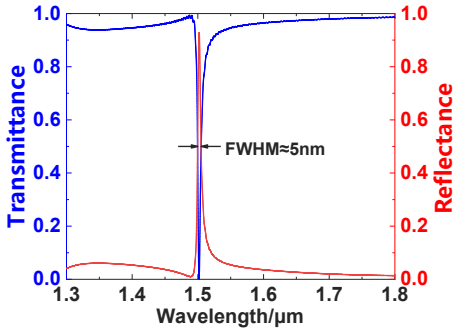

Fig. 2. Simulated transmission spectrum of the proposed structure when h = 0.5 μm, p = 1.1 μm, a = 0.21 μm, and l = 0.55 μm.

In our proposed minus filter, Si is a high refractive index material with a high transmittance in the near infrared region. To illustrate the underlying mechanism of the proposed minus filter, we carefully studied the electric (E) field and magnetic (H) fields at the resonance wavelengths. Figure 3(a)–(b) shows a transverse distribution chart of the E field and H field of the unit cell at a resonance wavelength of 1.49 μm. The E field is a vortex, and the H field is always parallel to the x-axis, which is typical of magnetic dipole (MD).

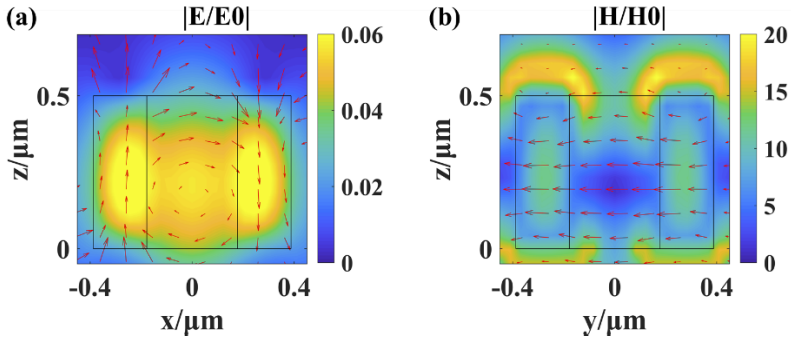

Fig. 3. (a) Electric field distributions at λ=1.5 μm in a unit cell in the x-z plane. (b) Magnetic field distributions at λ=1.49 μm in a unit cell in the y-z plane. The color bars stand for the normalized electric field and magnetic field intensity.

In principle, the unit cell of proposed structure can form an MD resonance and an electric dipole (ED) resonance. Different resonance modes that do not completely overlap will widen the spectrum width—this is not conducive to the formation of a narrow band. An effective solution is that we can separate the MD resonance from the ED sufficiently far to tune the MD alone

Optics EXPRESS

in the needed wavelength range. MD resonance is the basic mode and dominant mode of Mie resonance, and we can ignore the ED resonance in that the electric field will not appear in the wavelength range of consideration. Figure 4 shows that the simulated transmission spectrum of the proposed structure when the period of the unit cell changes from 1.5 μm to 1.1 μm. The distance between the MD resonance and ED resonance separates slowly, and we set the period of the unit cell to a fixed value (1.1 μm) so that we can tune the MD in the needed wavelength range.

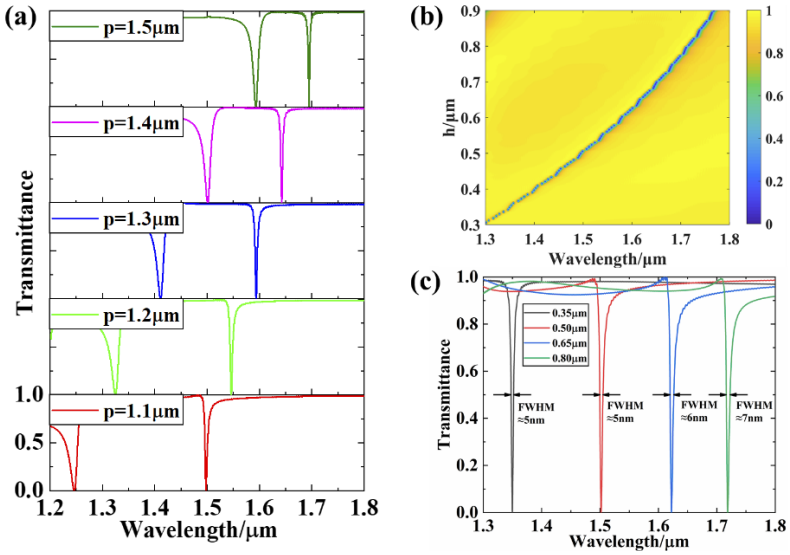

Fig. 4. (a) the simulated transmission spectrum of the proposed minus filter when p is set to 1.1 μm, 1.2 μm, 1.3 μm, 1.4 μm, and 1.5 μm. (b) the simulated transmission spectrum of the proposed minus filter with different h values. (c) the simulated transmission spectrum of the proposed minus filter when h is set to 0.35 μm, 0.5 μm, 0.65 μm, or 0.8 μm.

We next studied the tunability of the stop band around the proposed minus filter. We set the period of the structure to a fixed value of 1.1 μm and then the tunability of stopband was realized by changing the thickness of the structure. Figure 4(b) shows the sweep parameter diagram only by changing the thickness under a fixed period of 1.1 μm. When the thickness of the proposed structure varies from 0.3 μm to 0.9 μm, the position of stop band can be tuned from λ=1.3 μm to λ=1.8 μm. the transmittance of the stop band can always be maintained at 0, and the FWHM of the stopband is less than 10 nm. This performance is very beneficial to the design of narrow-band filter.

The angular dependence also needs to be considered when we design the minus filter. Figure 5(a) shows the transmission spectrum of the proposed minus filter at different angles (0, 10, 20, and 30) for x-polarization light. And we can see from the Partial enlargement spectrum figure of the stopband in the lower right corner of Fig. 5(a). Although the spectral transmission except the stop band decreases with the increasing angle, the position of the stop band does not shift at different angles (0, 10, 20, 30) for x-polarized light. Thus, if the incident angle is limited to a small range (less than 10), then the degradation of other wavelengths except the stop band is rather weak. Even if the incident angle is large, then the minus filter we proposed can precisely attenuate the light of stop band to a very low level.

Figure 5(b) presents the effects of polarization of the incident light. The symmetry of the structure will affect the sensitivity to polarization. The proposed structure is axisymmetric: The position of stopband remains unchanged when the polarization angle changed.

Optics EXPRESS

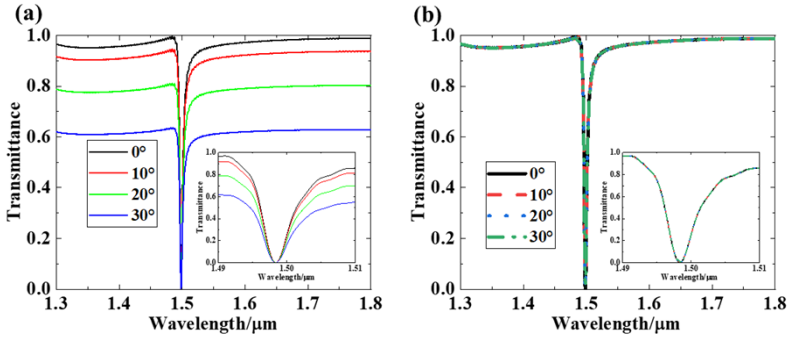

Fig. 5. (a) Transmission spectrum of the proposed minus filter at different angles (0, 10, 20, 30) for x-polarized light, (b) Transmission spectra of the proposed minus filter for incidents of light in different polarization directions. In the lower right of (a) and (b) is a partial enlargement spectrum figures of the stopband.

We also studied potential applications as a RI sensor. All dielectric RI sensors have great advantages in compared to early RI sensors based on metals [28–30]. For example, it is well known that the inherent loss of metal is not conducive to the formation of narrow band [31,32], resulting in low figure of merit (FOM) and quality factor (Q). And the composition of the tested sample will be changed due to local overheating [33–35]. Here we estimated several typical parameters of our proposed structure including RI range, sensing resolution, sensitivity, figure of merit (FOM) and quality factor (Q), which presents the performance of optical RI sensor. At first, the RI range and sensing resolution of the proposed structure were studied. Figure 6(a) shows the transmission spectrum of the proposed sensor when refractive index of the tested material changes from 1 to 1.7. We can see RI of the tested material has a liner relationship with the dip1 and dip2 of transmission spectrum. and the RI range is far beyond the above. Sensitivity (S) is a critical evaluating indicator of the RI sensor, which is usually defined by the following formula [36]: $S = (\Delta\lambda)/\Delta n$.

Here, $\Delta\lambda$ refer to the position offset of the resonance peak, Δn refer to the change of refractive index. The transmission spectra of the proposed structure were shown in Fig. 6(b) when RI of the tested materials changes from 1.3 to 1.35 with a change step of 0.005. The position of the dip1 and dip2 has moved significantly. Figure 6(c) shows relationship between the wavelength shift of dip1 and dip 2 and the RI of the tested materials. The small gray square and the small red circle respectively refers to the peak position of dip1 and dip2. Gray line and red line respectively refer to the fitted curve of dip1 and dip2. At the same time, it is also shown in the figure that S of the proposed structure are 953.53 nm/RIU of dip1 and 691.09 nm/RIU of dip2. S of the proposed structure significantly improved.

Finally, FOM and Q factor also were calculated to assess the performance of the proposed structure. The calculation formulas of the two parameters are as follows [37]: FOM = S/FWHM and Q=λ/FWHM. The FOM of dip1 and dip2 basically unchanged, which is 59.59 and 115.18. this is due to the FWHM of dip1 and dip 2 independent on the RI. Meanwhile, the position of dip1 and dip2 gradually red-shifted, resulting in that the Q of dip1 and dip2 increase slightly. Based on those estimation above mentioned, we considered the proposed structure exhibited a high performance, and hopeful application in RI sensor.

Optics EXPRESS

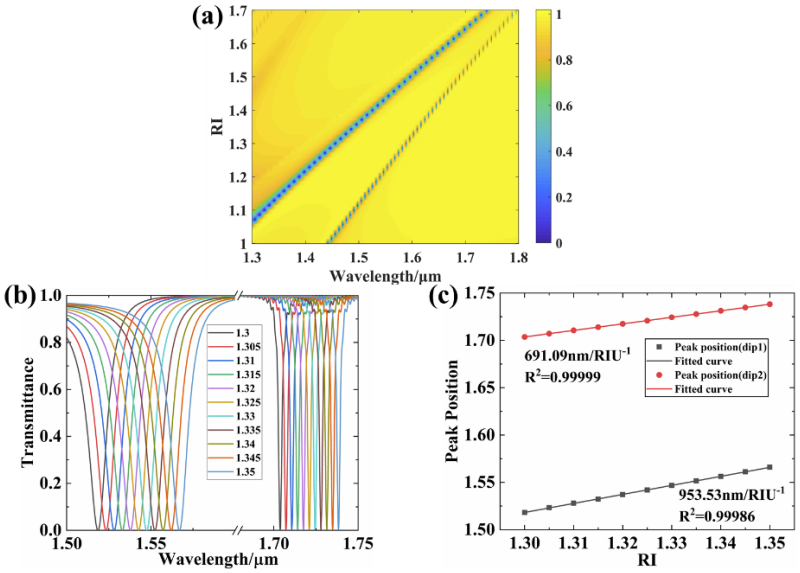

Fig. 6. (a) the transmission spectrum of the proposed sensor when refractive index of the tested material changes from 1 to 1.7. (b) The transmission spectra of the proposed structure when RI of the tested materials changes from 1.3 to 1.35 with a change step of 0.005. (c) Fitted curve between the wavelength shift of two resonance dips and the external refractive index

3. Conclusion

In summary, we have successfully designed an efficient narrow-band minus filter in near-infrared band by a proposed all-dielectric Si-SiO_2 bilayer structure. The FWHM of its stop band is just 5 nm, whose transmittance is close to 0, whereas its broad pass band transmittance is as high as 90% in the work wavelength range. We also clarified the influence of geometric parameters on the filtering characteristics and proved the convenience of designing the desired minus filter by adjusting the thickness of silicon layer. By analyzing the electric field and magnetic field of the structure, it can be clearly concluded that this phenomenon originates from magnetic dipole resonance, and the proposed structure is insensitive to change of incident light angle and polarization angle. Additionally, we studied its potential application on refractive index sensor. Its sensitivity of dip1 and dip2 are as high as 953.53 nm/RIU and 691.09nm/RIU, while their figure of merit is almost unchanged, maintaining 59.59 and 115.18, respectively.

Funding. The Science and Technology Innovation Project of Jilin Province and Chinese Academy of Sciences (2020SYHZ0007); National Natural Science Foundation of China (62005272, 61875193).

Disclosures. The authors declare no conflicts of interest.

Data availability. Data underlying the results presented in this paper are not publicly available at this time but maybe obtained from the authors upon reasonable request.

References

1. J. A. Dobrowolski, *Handbook of Optics: Fundamentals, Techniques, and Design*, Volume I, 2nd Edition (Academic, 1995), Chap.11.
2. J. Minguillon, M. A. Lopez-Gordo, D. A. Renedo-Criado, M. J. Sanchez-Carrion, and F. Pelayo, "Blue lighting accelerates post-stress relaxation: Results of a preliminary study," PLoS One **12**(10), e0186399 (2017).
3. C. C. Lee, "Optical interference coatings for optics and photonics [Invited]," Appl. Opt. **52**(1), 73–81 (2013).
4. J. Zhang, G. Sen, and X. Li, "Design of Optical Notch Filters Based on Equivalent Relations," Adv. Mater. Res. **679**, 47–52 (2013).

Optics EXPRESS

5. J. Yan, X. Q. Zheng, W. M You, W. X. He, and G. K. Xu, "A Bionic-Homodimerization Strategy for Optimizing Modulators of Protein-Protein Interactions: From Statistical Mechanics Theory to Potential Clinical Translation," Adv. Sci. (to be published).
6. J. Versna, L. Marc, G. Bjoern, R. Detlev, S. Uwe, S. Olaf, and K. Norbert, "Comparison of gradient index and classical designs of a narrow band notch filter," Proc. SPIE **5963**, 59631O (2005).
7. R. W. Sprague, B. Shnapir, and G. L. Minott, "Rugate notch filters find use in laser-based applications," Laser Focus World **40**(9), 107–111 (2004).
8. X. L. Zhang, Y. B. Tang, F. Zhang, and C. S. Lee, "A Novel Aluminum-Graphite Dual-Ion Battery," Adv. Energy Mater. **6**(11), 1502588 (2016).
9. M. Wang, C. L. Jiang, S. Q. Zhang, X. H. Song, and Y. B. Tang, "Reversible calcium alloying enables a practical room-temperature rechargeable calcium-ion battery with a high discharge voltage," Nat. Chem. **10**(6), 667–672 (2018).
10. C. L. Holloway, E. F. Kuester, J. A. Gordon, J. O'Hara, J. Booth, and D. R. Smith, "An Overview of the Theory and Applications of Metasurfaces: The Two-Dimensional Equivalents of Metamaterials," IEEE Trans. Antennas Propag. **54**(2), 10–35 (2012).
11. A. Kildishev, A. Boltasseva, and V. Shalaev, "Planar Photonics with Metasurfaces," Science **339**(6125), 1289–1296 (2013).
12. N. F. Yu, P. Genevet, M. A. Kats, F. Aieta, J. P. Tetienne, F. Capasso, and Z. Gaburro, "Light Propagation with Phase Discontinuities: Generalized Laws of Reflection and Refraction," Science **334**(6054), 333–337 (2011).
13. N. F. Yu and F. Capasso, "Flat optics with designer metasurfaces," Nat. Mater. **13**(2), 139–150 (2014).
14. O. Hess, J. B. Pendry, S. A. Maier, R. F. Oulton, J. M. Hamm, and K. L. Tsakmakidis, "Active nanoplasmonic metamaterials," Nat. Mater. **11**(7), 573–584 (2012).
15. X. J. Huang, X. Ma, X. W. Li, J. D. Fan, L. Guo, and H. L. Yang, "Simultaneous realization of polarization conversion for reflected and transmitted waves with bi-functional metasurface," Sci. Rep. **12**(1), 2368–2378 (2022).
16. Y. H. Gu, L. Zhang, J. K. W. Yang, S. P. Yeo, and C. W. Qiu, "Color generation *via* subwavelength plasmonic nanostructures," Nanoscale **7**(15), 6409–6419 (2015).
17. S. Yokogawa, S. P. Burgos, and H. A. Atwater, "Plasmonic Color Filters for CMOS Image Sensor Applications," Nano Lett. **12**(8), 4349–4354 (2012).
18. S. P. Burgos, S. Yokogawa, and H. A. Atwater, "Color Imaging *via* Nearest Neighbor Hole Coupling in Plasmonic Color Filters Integrated onto a Complementary Metal-Oxide Semiconductor Image Sensor," ACS Nano **7**(11), 10038–10047 (2013).
19. J. B. Gao, J. S. Gao, Z. Z. Li, H. G. Yang, H. Liu, X. Y. Wang, T. T. Wang, K. Wang, Q. Li, X. Y. Liu, Y. C. Wang, R. Q. Gao, and Y. H. Zhao, "Linewidth reduction effect of a cavity-coupled dual-passband plasmonic filter," Opt. Express **28**(6), 8753–8763 (2020).
20. J. B. Gao, J. S. Gao, H. G. Yang, H. Liu, X. Y. Wang, K. Wang, X. Y. Liu, Q. Li, Y. C. Wang, Z. Z. Li, R. Q. Gao, and Z. Zhang, "Cavity-driven hybrid plasmonic ultra-narrow bandpass filter," Opt. Express **27**(15), 20397–20411 (2019).
21. T. Xu, Y. K. Wu, X. G. Luo, and L. J. Guo, "Plasmonic nanoresonators for high-resolution colour filtering and spectral imaging," Nat Commun **1**(1), 59–64 (2010).
22. D. Fleischman, L. A. Sweatlock, H. Murakami, and H. Atwater, "Hyper-selective plasmonic color filters," Opt. Express **25**(22), 27386–27395 (2017).
23. R. C. Ng, J. C. Garcia, J. R. Greer, and K. T. Fountaine, "Polarization-Independent, Narrowband, Near-IR Spectral Filters via Guided Mode Resonances in Ultrathin a-Si Nanopillar Arrays," ACS Photonics **6**(2), 265–271 (2019).
24. M. Niraula, J. W. Yoon, and R. Magnusson, "Single-layer optical bandpass filter technology," Opt. Lett. **40**(21), 5062–5065 (2015).
25. B. Yang, W. W. Liu, Z. C. Li, H. Cheng, D. Y. Choi, S. Q. Chen, and J. G. Tian, "Ultrahighly Saturated Structural Colors Enhanced by Multipolar-Modulated Metasurfaces," Nano Lett. **19**(7), 4221–4228 (2019).
26. C. Y. Yang, Z. Wang, H. X. Yuan, K. Li, X. W. Zheng, W. Mu, W. J. Yuan, Y. G. Zhang, and W. D. Shen, "All-Dielectric Metasurface for Highly Tunable, Narrowband Notch Filtering," IEEE Photonics J. **11**(4), 1–6 (2019).
27. E. D. Palik, *Handbook of optical constant of solids* (Academic, 1997).
28. A. V. Kabashin, P. Evans, S. Pastkovsky, W. Hendren, G. A. Wurtz, R. Atkinson, R. Pollard, V. A. Podolskiy, and A. V. Zayats, "Plasmonic nanorod metamaterials for biosensing," Nature Mater **8**(11), 867–871 (2009).
29. N. Liu, M. Mesch, T. Weiss, M. Hentschel, and H. Giessen, "Infrared Perfect Absorber and Its Application as Plasmonic Sensor," Nano Lett. **10**(7), 2342–2348 (2010).
30. P. L. Xu, L. G. Cui, S. W. Gao, N. Na, and A. G. Ebadi, "A theoretical study on sensing properties of in-doped ZnO nanosheet toward acetylene," Mol Phys (to be published).
31. D. U. Yildirim, A. Ghobadi, M. C. Soydan, O. Atesal, A. Toprak, M. D. Caliskan, and E. Ozbay, "Disordered and Densely Packed ITO Nanorods as an Excellent Lithography-Free Optical Solar Reflector Metasurface," ACS Photonics **6**(7), 1812–1822 (2019).
32. M. C. Soydan, A. Ghobadi, D. U. Yildirim, V. B. Erturk, and E. Ozbay, "All Ceramic-Based Metal-Free Ultra-broadband Perfect Absorber," Plasmonics **14**(6), 1801–1815 (2019).
33. N. Bontempi, K. E. Chong, H. W. Orton, I. Staude, D. Y. Choi, I. Alessandri, Y. S. Kivshar, and D. N. Neshev, "Highly sensitive biosensors based on all-dielectric nanoresonators," Nanoscale **9**(15), 4972–4980 (2017).

Optics EXPRESS

34. O. Yavas, M. Svedendahl, P. Dobosz, V. Sanz, and R. Quidant, "On-a-chip Biosensing Based on All-Dielectric Nanoresonators," Nano Lett. **17**(7), 4421–4426 (2017).
35. M. Mahmoudi, S. E. Lohse, C. J. Murphy, A. Fathizadeh, A. Montazeri, and K. S. Suslick, "Variation of Protein Corona Composition of Gold Nanoparticles Following Plasmonic Heating," Nano Lett. **14**(1), 6–12 (2014).
36. Y. Cao, H. Y. Liu, Z. R. Tong, S. Yuan, and S. Zhao, "Simultaneous measurement of temperature and refractive index based on a core-offset Mach-Zehnder interferometer cascaded with a long-period fiber grating," Optoelectron. Lett. **11**(1), 69–72 (2015).
37. Y. Xu, P. Bai, X. Zhou, Y. Akimov, C. E. Png, L. K. Ang, W. Knoll, and L. Wu, "Optical Refractive Index Sensors with Plasmonic and Photonic Structures: Promising and Inconvenient Truth," Adv. Opt. Mater. **7**(9), 1801433 (2019).